

# A Sensor-less Surface Mounted PMSM for Electronic Speed Control in Multilevel Inverter

S. Dinesh Kumar<sup>1,\*</sup> and A. Jagadeeshwaran<sup>2</sup>

<sup>1</sup>Karthikeya Polytechnic College, Manapparai, Tamil Nadu, 621306, India

<sup>2</sup>Department of Electrical and Electronics Engineering, Sona College of Technology, Salem, Tamil Nadu, 636005, India

\*Corresponding Author: S. Dinesh Kumar. Email: sdkeee@gmail.com

Received: 18 January 2022; Accepted: 27 March 2022

**Abstract:** Recent advancements in power electronics technology evolves inverter fed electric motors. Speed signals and rotor position are essential for controlling an electric motor accurately. In this paper, the sensorless speed control of surface-mounted permanent magnet synchronous motor (SPMSM) has been attempted. SPMSM wants a digital inverter for its precise working. Hence, this study incorporates fifteen level inverter to the SPMSM. A sliding mode observer (SMO) based sensorless speed control scheme is projected to determine rotor spot and speed of the multilevel inverter (MLI) fed SPMSM. MLI has been operated using a multi carrier pulse width modulation (MCPWM) strategy for generation of fifteen level voltages. The simulation works are executed with MATLAB/SIMULINK software. The steadiness and the heftiness of the projected model have been investigated under no loaded and loaded situations of SPMSM. Furthermore, the projected method can be adapted for electric vehicles.

**Keywords:** Surface-mounted permanent magnet synchronous motor; sensorless speed control; multilevel inverter; torque estimation; multi carrier pulse width modulation

## 1 Introduction

PMSM has been used broadly because of its advantageous features such as better power density, good torque ratio, worthy efficacy, minimum loss and compact [1,2]. By the placement of the permanent magnet on the rotor, PMSM has been classified into two categories such as SPMSM and interior PMSM (IPMSM). SPMSM has identical direct and quadrature axis inductances; on the other hand, IPMSM partakes the uneven direct and quadrature axis inductances. So as to achieve precise control of SPMSM, the data of rotor spot and speed have been required. Conventionally mechanical sensors were employed to find the rotor spot and speed. They have several disadvantages such as high cost, increased size, decreased reliability and minimized applications [3]. To overwhelm those drawbacks, the sensorless control scheme for PMSM has been proposed [4,5]. Then various control schemes for instance space vector control [6], direct torque control [7], model reference adaptive system (MRAS) [8] have been presented. The vector control system is accurate, dynamic and has extensive limit of speed and spot control. Continually, the intelligent



This work is licensed under a Creative Commons Attribution 4.0 International License, which permits unrestricted use, distribution, and reproduction in any medium, provided the original work is properly cited.



technique namely neural network (NN) has been proposed to design the speed controller for PMSM [9]. It has the merits of quick convergence rate, great exactness and robust.

Recently, various sensorless control and state estimation techniques have been projected [10–12]. Among them SMO and MRAS based sensorless control strategies have been utilized more. Because, they can be implemented easily in the digital systems and has the merits of simplicity and rapid control. A fuzzy based controller scheme has been proposed to replace the Proportional–Integral–Derivative (PID) controller in MRAS [13]. An adaptive line enhancer along with SMO scheme has been introduced to increase the reference ideal for the speed auto-sensing of an IPMSM [14]. An advanced SMO scheme has been presented to control speed in a fuzzy controlled wind energy conversion system [15]. The stability investigation of sensorless speed control strategy for PMSM using MRAS has been performed [16]. To minimize the opposing influence of stricture disparity in sensorless speed control of a PMSM, the multiple stricture assessment by means of MRAS has been presented [17]. The modelling and simulation of a novel brain emotional learning and fuzzy-based intelligent controller (BELFBIC) for 3 phase induction motor V/f speed control was proposed [18], and it has been tested [19,20]. Lately, the authors have carried out a study on a sensorless T-source inverter-based PMSM drive incorporating the PI controller along with a technique to handle the time-altering strictures [21]. This study intends a sensorless speed control scheme using SMO for a SPMSM. It intends to legalize the rotor speed according to the change in load torque. In Section 2, the exact prototypical of MLI fed SPMSM has been presented. Section 3 discusses the SMO based sensorless control scheme to evaluate the rotor position and the speed. Section 4 provides the simulation results and Section 5 accomplishes the study.

## 2 Modelling of SPMSM

The structure of a SPMSM has been demonstrated in Fig. 1. In a SPMSM,  $L_d = L_q = L$ . Thus in the two-phase revolving  $d$ - $q$  direct, the voltage equations of SPMSM have been provided.

$$u_d = Ri_d + L \frac{di_d}{dt} - Lp\omega i_q \quad (1)$$

$$u_q = Ri_q + L \frac{di_q}{dt} + Lp\omega i_d + \psi_f p\omega \quad (2)$$

where

$i_d, i_q$	current in $d$ and $q$ axis
$u_d, u_q$	voltage in $d$ and $q$ axis
$L$	inductance
$R$	resistance
$\psi_f$	magnetic flux
$\omega$	rotor speed
$p$	no. of pole pairs

The machine-driven movement of SPMSM can be expressed from Eqs. (3) and (4).

$$\frac{d\theta}{dt} = \omega \quad (3)$$

$$\frac{d\omega}{dt} = \frac{1}{J}(T - F\omega - T_L) \quad (4)$$

where



- $\theta$  rotor spot  
 $J$  moment of inertia  
 $T$  motor torque  
 $F$  viscous friction constant  
 $T_L$  load torque

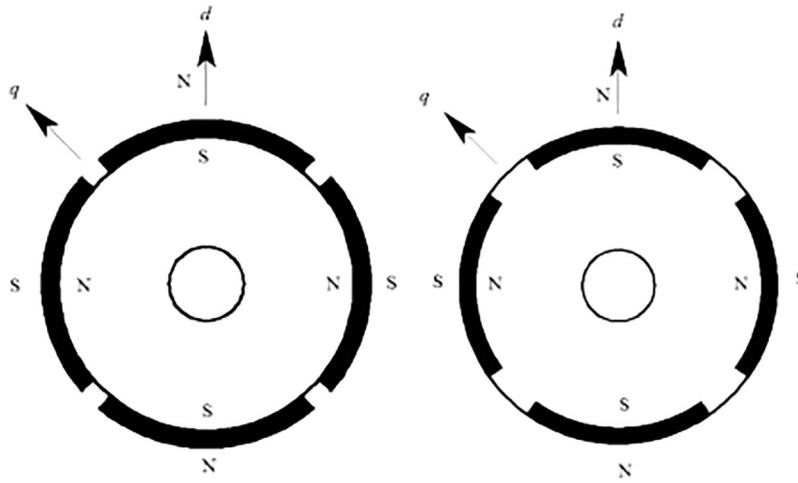


**Figure 1:** Assembly of SPMSM

The vector control scheme controls the motor current using stator current vector and magnetic field coordination standard. Consequently, the motor torque has been controlled. In SPMSM, the vector control system  $i_d = 0$ .

The torque equation of SPMSM has been expressed in Eq. (5).

$$T = \frac{3}{2} p \psi_f i_q \quad (5)$$

Torque  $T$  is directly proportional to the current  $i_q$ . For controlling the torque, the current  $i_q$  has to be altered. The adaptation association amid the 2 phase revolving  $d - q$  direct system and 2 phase stationary  $\alpha - \beta$  direct system has been illustrated in Fig. 2.

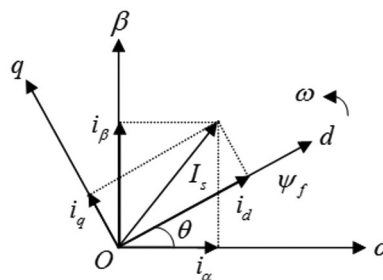


**Figure 2:** Conversion illustration amid the 2 coordinate system

The Park's converse conversion has been presented to convert the  $d-q$  mount that revolves beside the untrue excitation vector  $i_f$  absorbed as the  $d$  axis into the static stator  $\alpha - \beta$  mount.



$$P = \begin{bmatrix} \cos(p\theta) & -\sin(p\theta) \\ \sin(p\theta) & \cos(p\theta) \end{bmatrix} \quad (6)$$

The modelling of SPMSM in the 2 phase fixed  $\alpha - \beta$  orientation mount have been expressed as

$$\frac{di_\alpha}{dt} = -\frac{Ri_\alpha}{L} - \frac{e_\alpha}{L} + \frac{u_\alpha}{L} \quad (7)$$

$$\frac{di_\beta}{dt} = -\frac{Ri_\beta}{L} - \frac{e_\beta}{L} + \frac{u_\beta}{L} \quad (8)$$

$$e_\alpha = -\psi_f p \omega \sin(p\theta) \quad (9)$$

$$e_\beta = \psi_f p \omega \cos(p\theta) \quad (10)$$

$$T = \frac{3}{2} p \psi_f [-i_\alpha \sin(p\theta) + i_\beta \cos(p\theta)] \quad (11)$$

where

- $i_\alpha, i_\beta$  current for individual phase
- $u_\alpha, u_\beta$  voltage for individual phase
- $e_\alpha, e_\beta$  back EMF for individual phase
- $L$  inductance
- $R$  resistance
- $\psi_f$  magnetic flux
- $\omega$  rotor speed
- $\theta$  rotor position

The structure of SMO based sensorless speed control for MLI fed SPMSM has been displayed in [Fig. 3](#).

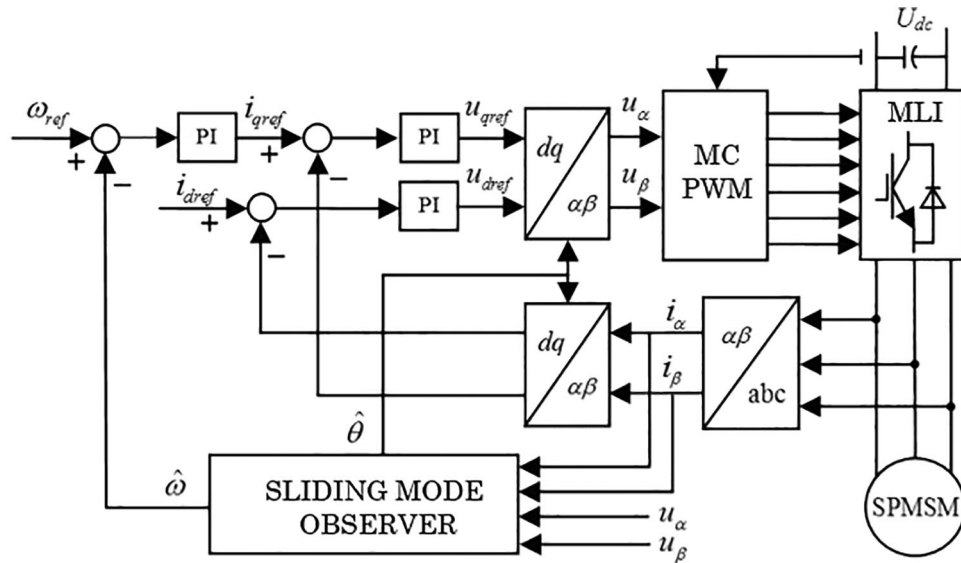


**Figure 3:** Illustration of SMO based sensorless speed control scheme for MLI fed SPMSM



## 2.1 Fifteen-Level MLI

MLI have an organization of power switching devices and capacitor voltage sources. MLI are apt for high-voltage applications due to their capability to produce output voltage waveforms with an improved harmonic band and get greater voltages with a minimum device ranking. MLI have the capability to satisfy the growing demand of power rating and power quality. The circuit diagram of the 1 phase 15-level MLI is exposed in Fig. 4.

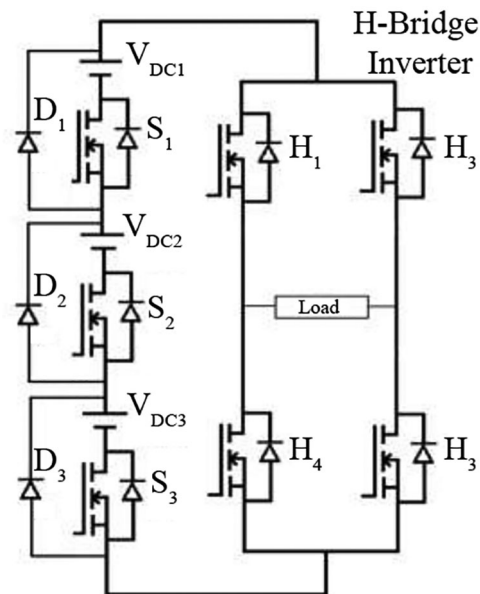


**Figure 4:** Circuit diagram of the single phase 15-level MLI

The 1-phase 15-level inverter has been established from the 7-level inverter. It involves a 1-phase traditional H-bridge inverter, 3 switches, and 3 voltage sources. The H-bridge methodology has the advantages such as minimized count of switches, diodes for inverters of the similar count of levels. Appropriate switching of MLI can generate 15 output voltage levels such as  $V_{dc}$ ,  $6 V_{dc}/7$ ,  $5 V_{dc}/7$ ,  $4 V_{dc}/7$ ,  $3 V_{dc}/7$ ,  $2 V_{dc}/7$ ,  $V_{dc}/7$ ,  $0$ ,  $-V_{dc}/7$ ,  $-2 V_{dc}/7$ ,  $-3 V_{dc}/7$ ,  $-4 V_{dc}/7$ ,  $-5 V_{dc}/7$ ,  $-6 V_{dc}/7$ ,  $-V_{dc}$  from the dc supply voltage. In this paper, multi carrier pulse width modulation (MCPWM) method has been employed to create the fifteen level output voltage as shown in Fig. 5.

Seven equivalent heft carrier triangular signals with compensation is likened with the sinusoidal reference pulse. They have been applied to the switches  $S_1$ ,  $S_2$ ,  $S_3$ . After these 2 sinusoidal pulses with  $180^\circ$  shift have been likened with the carrier triangular pulse. These PWM pulses consists of dead band and it will evade the discharge over issue amid two components. These PWM signals have been applied to the 1-phase inverter circuit switches  $H_1$ ,  $H_2$ ,  $H_3$ , and  $H_4$ . It has been experienced that the controlling of DC buses is simple while using MLI. Fig. 6 demonstrates the switching patterns of PV system based 15-level single phase MLI output voltage.



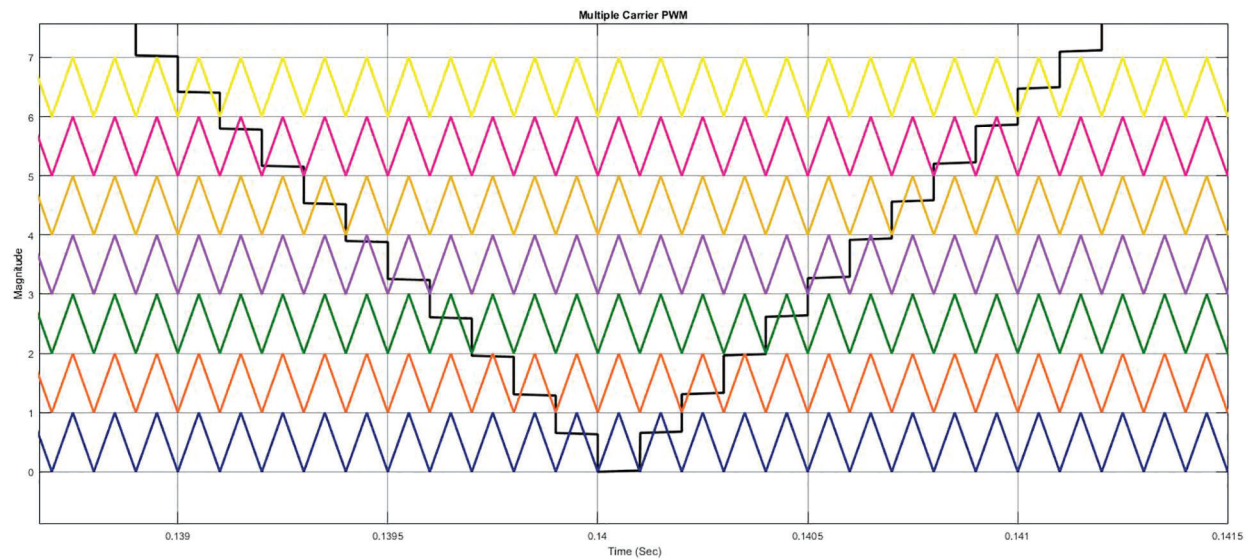


Figure 5: Waveform of MCPWM

S.No	S <sub>1</sub>	S <sub>2</sub>	S <sub>3</sub>	H <sub>1</sub>	H <sub>2</sub>	H <sub>3</sub>	H <sub>4</sub>	Output voltage
1	ON	ON	ON	ON	ON	OFF	OFF	$V_{dc}$
2	ON	ON	ON	ON	ON	OFF	OFF	$6/7V_{dc}$
3	ON	ON	OFF	ON	ON	OFF	OFF	$5/7V_{dc}$
4	ON	OFF	ON	ON	ON	OFF	OFF	$4/7V_{dc}$
5	ON	OFF	OFF	ON	ON	OFF	OFF	$3/7V_{dc}$
6	OFF	ON	OFF	ON	ON	OFF	OFF	$2/7V_{dc}$
7	OFF	OFF	ON	ON	ON	OFF	OFF	$1/7V_{dc}$
8	OFF	OFF	OFF	OFF	OFF	OFF	OFF	0
9	OFF	OFF	ON	OFF	OFF	ON	ON	$-1/7V_{dc}$
10	OFF	ON	OFF	OFF	OFF	ON	ON	$-2/7V_{dc}$
11	ON	OFF	OFF	OFF	OFF	ON	ON	$-3/7V_{dc}$
12	ON	OFF	ON	OFF	OFF	ON	ON	$-4/7V_{dc}$
13	ON	ON	OFF	OFF	OFF	ON	ON	$-5/7V_{dc}$
14	ON	ON	ON	OFF	OFF	ON	ON	$-6/7V_{dc}$
15	ON	ON	ON	OFF	OFF	ON	ON	$-V_{dc}$

Figure 6: Switching pattern for 15-level 7-switch topology



### 3 Modelling of SMO

In the  $\alpha - \beta$  coordination, the electrical equation of SPMSM can be expressed as follows.

$$\frac{dx}{dt} = A_{EI}x + B_{\gamma}u \quad (12)$$

$$y = C_I x \quad (13)$$

$$x = [i_{\alpha} \quad i_{\beta} \quad e_{\alpha} \quad e_{\beta}] \quad (14)$$

$$u = \begin{bmatrix} u_{\alpha} \\ u_{\beta} \end{bmatrix} \quad (15)$$

$$A_{EI} = \begin{bmatrix} A & B \\ 0 & D \end{bmatrix} \quad (16)$$

$$B_{\gamma} = \begin{bmatrix} -B \\ 0 \end{bmatrix} \quad (17)$$

$$C_I = [C \quad 0] \quad (18)$$

$$A = \begin{bmatrix} \frac{-R_s}{L_s} & 0 \\ 0 & \frac{-R_s}{L_s} \end{bmatrix} \quad (19)$$

$$B = \begin{bmatrix} \frac{1}{L_s} & 0 \\ 0 & \frac{1}{L_s} \end{bmatrix} \quad (20)$$

$$D = \begin{bmatrix} 0 & -\omega_r \\ \omega_r & 0 \end{bmatrix} \quad (21)$$

$$i_s = \begin{bmatrix} i_{\alpha} \\ i_{\beta} \end{bmatrix} \quad (22)$$

$$e_s = \begin{bmatrix} e_{\alpha} \\ e_{\beta} \end{bmatrix} \quad (23)$$

where  $e_{\alpha}$ ,  $e_{\beta}$  are the electrical motive force.

The dynamic error equations of SPMSM can be given as follows.

$$\frac{d\tilde{i}_s}{dt} = A\tilde{i}_s + B\tilde{e}_s - K_1 \text{sgn}(\tilde{i}_s) \quad (24)$$

$$\frac{d\tilde{e}_s}{dt} = \tilde{D}\tilde{e}_s + l_1 K_1 \text{sgn}(\tilde{i}_s) \quad (25)$$



where

$$\tilde{D} = \begin{bmatrix} 0 & \tilde{\omega}_r \\ -\tilde{\omega}_r & 0 \end{bmatrix} \quad (26)$$

The sliding mode has been defined as

$$\tilde{i}_s = \frac{d\tilde{i}_s}{dt} = 0 \quad (27)$$

On the sliding mode,

$$\frac{d\tilde{e}_\alpha}{dt} = \tilde{\omega}_r \tilde{e}_\beta + l_2 \tilde{e}_\alpha \quad (28)$$

$$\frac{d\tilde{e}_\beta}{dt} = -\tilde{\omega}_r \tilde{e}_\alpha + l_2 \tilde{e}_\beta \quad (29)$$

The Lyapunov function has been characterized as

$$V = \frac{1}{2} (\tilde{e}_\alpha^2 + \tilde{e}_\beta^2 + \tilde{\omega}_r^2) \quad (30)$$

$$\frac{dV}{dt} = \tilde{e}_\alpha \frac{d\tilde{e}_\alpha}{dt} + \tilde{e}_\beta \frac{d\tilde{e}_\beta}{dt} + \tilde{\omega}_r \frac{d\tilde{\omega}_r}{dt} < 0 \quad (31)$$

The substitution of Eqs. (29) and (30) into (31) offers

$$\frac{d\tilde{\omega}_r}{dt} = \tilde{e}_\alpha \tilde{e}_\beta - \tilde{e}_\beta \tilde{e}_\alpha \quad (32)$$

The rotor position and speed have been assessed as

$$\tilde{\omega}_r = \left( \frac{K_i}{p + K_p} \right) \varepsilon \quad (33)$$

$$\hat{\theta} = \int \hat{\omega} dt \quad (34)$$

where

$$\varepsilon = \tilde{e}_\alpha \tilde{e}_\beta - \tilde{e}_\beta \tilde{e}_\alpha \quad (35)$$

## 4 Simulation Results

The specifications of SPMSM for simulation are provided in Tab. 1. The MATLAB simulink model is exemplified in Fig. 7.

The results have been attained for 2 dissimilar situations for instance no load and loaded settings with the established model. In both conditions, the simulation is executed for four dissimilar reference speeds for instance 670, 800, 750, 1000 and 1500 rpm.

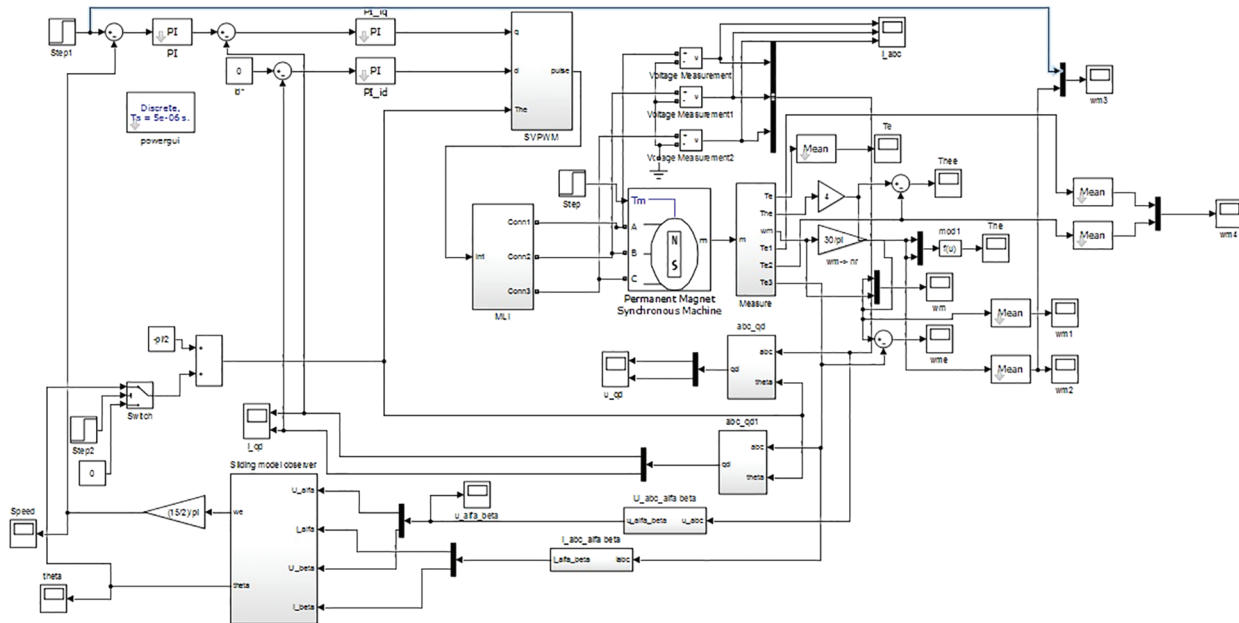
### 4.1 Case 1: No Load Situation

Here the load has not been connected. The simulation outcomes are extracted for 4 dissimilar reference speeds. Fig. 8 demonstrates the speed waveform along with reference and output speed signs for 670, 800, 1000 and 1500 rpm respectively. Correspondingly, the torque waveform attained for the aforesaid speeds has been exposed in Fig. 9.



**Table 1:** Strictures of SPMSM

Strictures	Notation	Values
Regarded speed	$\omega_r$	1200 rpm
Rated power	$P_{rated}$	750 W
Regarded phase voltage	$V_{ph}$	220 V
Regarded phase current	$I_{ph}$	4.3 A
Regarded torque	$T_{rated}$	3.10 Nm
No. of poles	$P$	4
Resistance of stator	$R_s$	0.43 ohm
Inductance of stator	$L_s$	3.2 mH
Magnetic flux	$Y_{af}$	0.085 Vs/rad
Equal inertia	$J$	0.004 kg/m <sup>2</sup>
Viscous friction constant	$B$	0.0002 Nm.s/rad

**Figure 7:** Simulink prototype of the projected system

From the Figs. 8 and 9, it has been identified that, the speed of the SPMSM slow down down at 0.05 s for least speeds, while the identical at 0.1 s for high speeds with a minor primal perturbation. The output speeds of the SPMSM evidently portrays that, it has not noticeable fluctuations that is vastly favored for several perpetual appliances. For no load situation, the torque will be 0 Nm. At the speed of 0 rpm, the torque will be 0 Nm. Conversely, at higher speeds the torque has specific primal fluctuations and slow down to 0 Nm finally. The fluctuations are at the bound of 0.02, 0.02, 0.03 and 0.09 Nm for the speed ranges 670, 800, 1000 and 1500 rpm respectively. The current waveform of d and q axis has been illustrated in Fig. 10. Similarly, the stator current waveform under no loaded condition has been shown in Fig. 11.



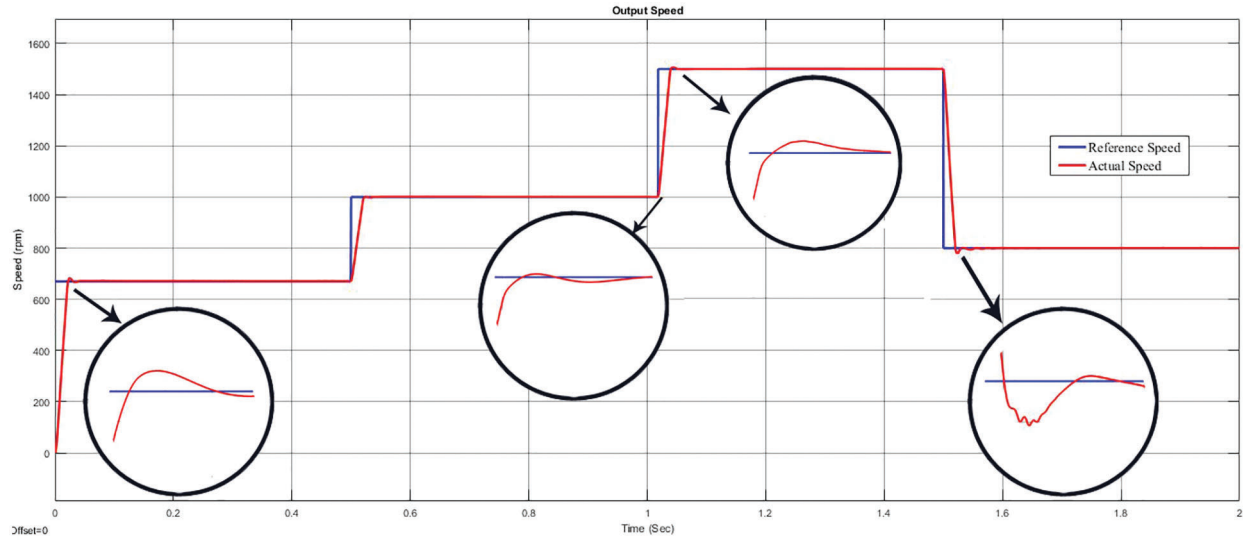


**Figure 8:** Output speed waveform with reference and actual speeds under no loaded condition

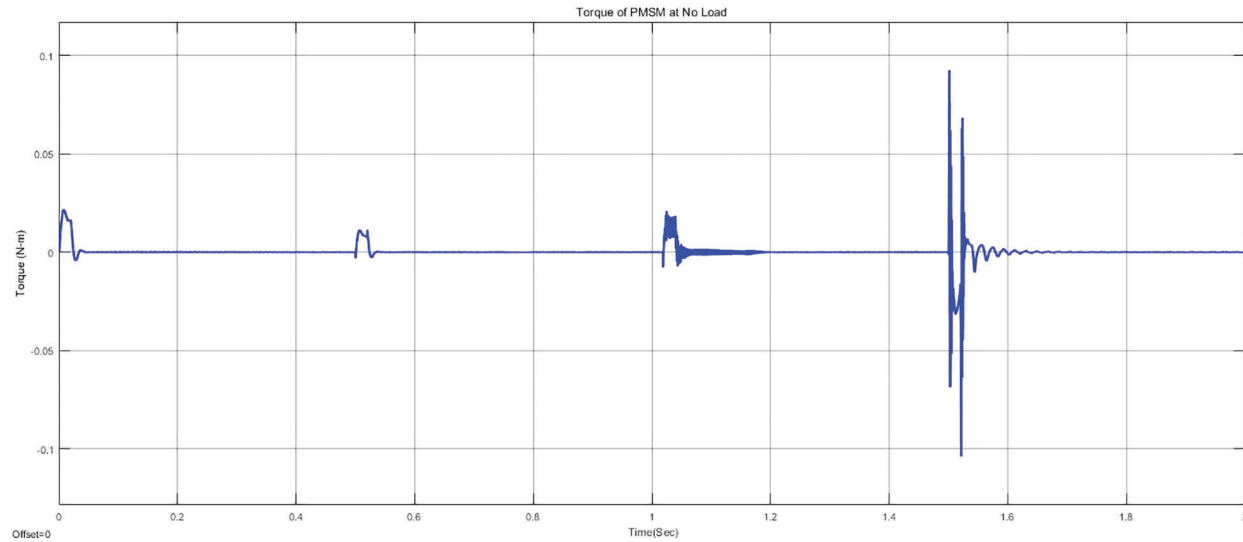


**Figure 9:** Output torque waveform under no loaded condition

#### 4.2 Case 2: Loaded Condition

In this case, a load of 3 Nm has been connected at the running condition during 0.4 and 1.5 s. A minor deviance amid the reference and output speed has been occurred. The speed response waveforms have been illustrated in Fig. 12. The respective torque waveform has been shown in Fig. 13. The current waveform of d and q axis under loaded condition has been illustrated in Fig. 14. Similarly, the stator current waveform under loaded condition has been shown in Fig. 15.

The advantage of the proposed method is albeit at loaded situation, the anticipated output speed has been attained without any significant fluctuations. Likewise, the torque waveform has no ripple content, thus the efficacy of SPMSM has been improved. It results with the noiseless operation of SPMSM.



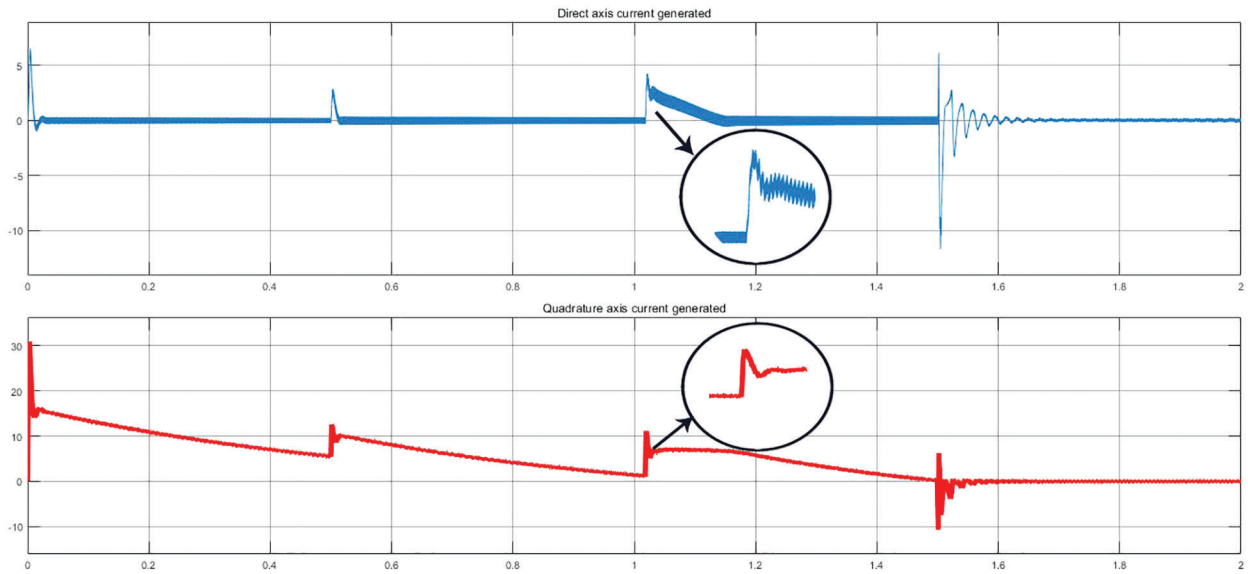


**Figure 10:** Current waveform of d and q axis under no loaded condition

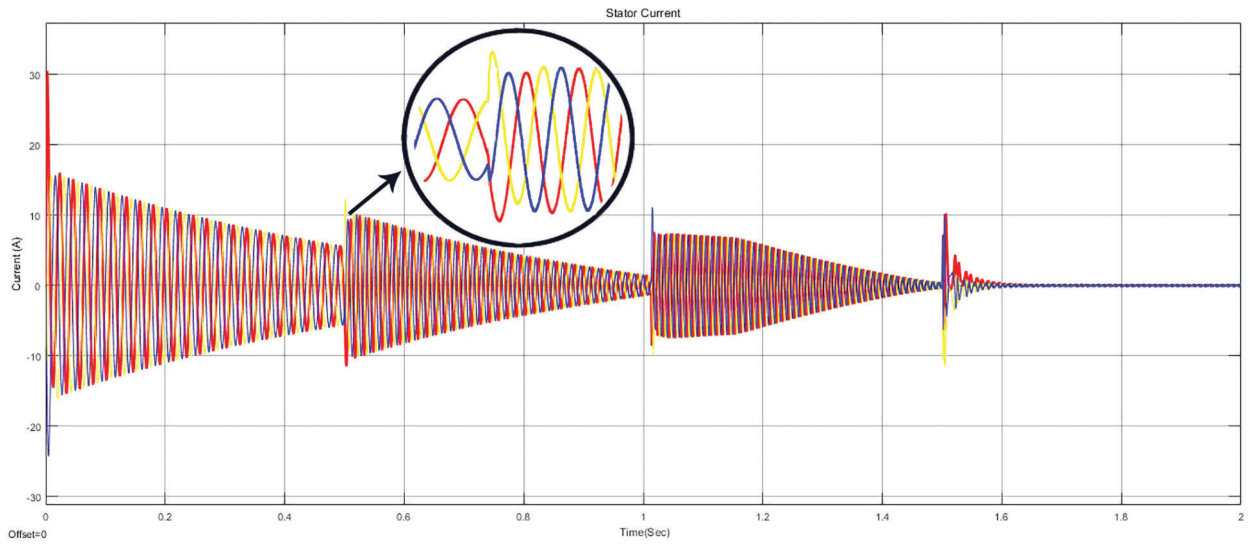


**Figure 11:** Stator current waveform under no loaded condition



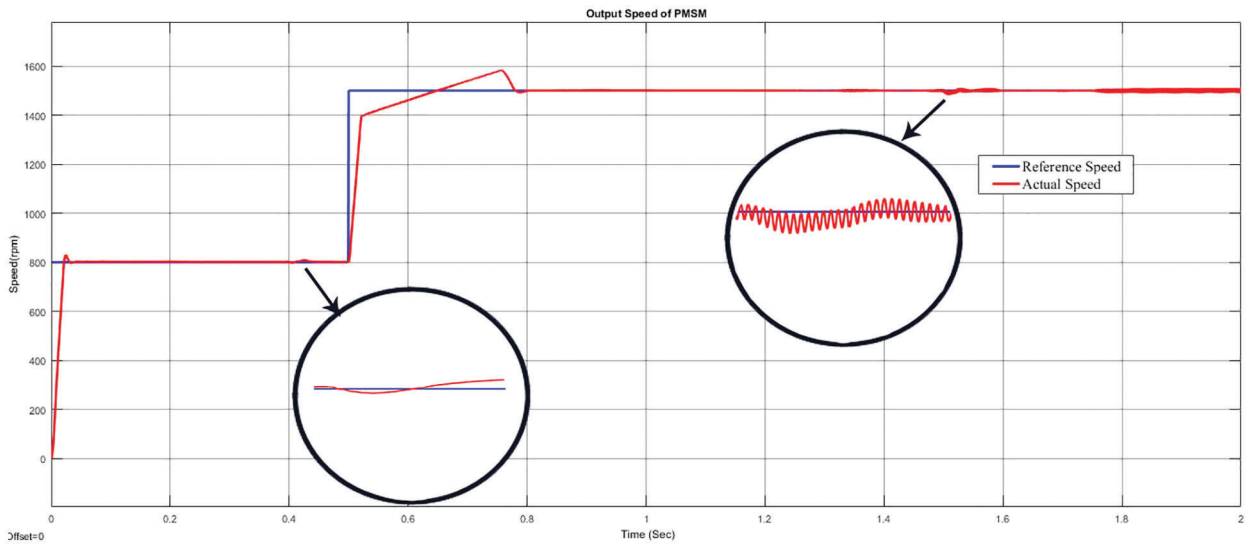


Figure 12: Output speed waveform under loaded condition

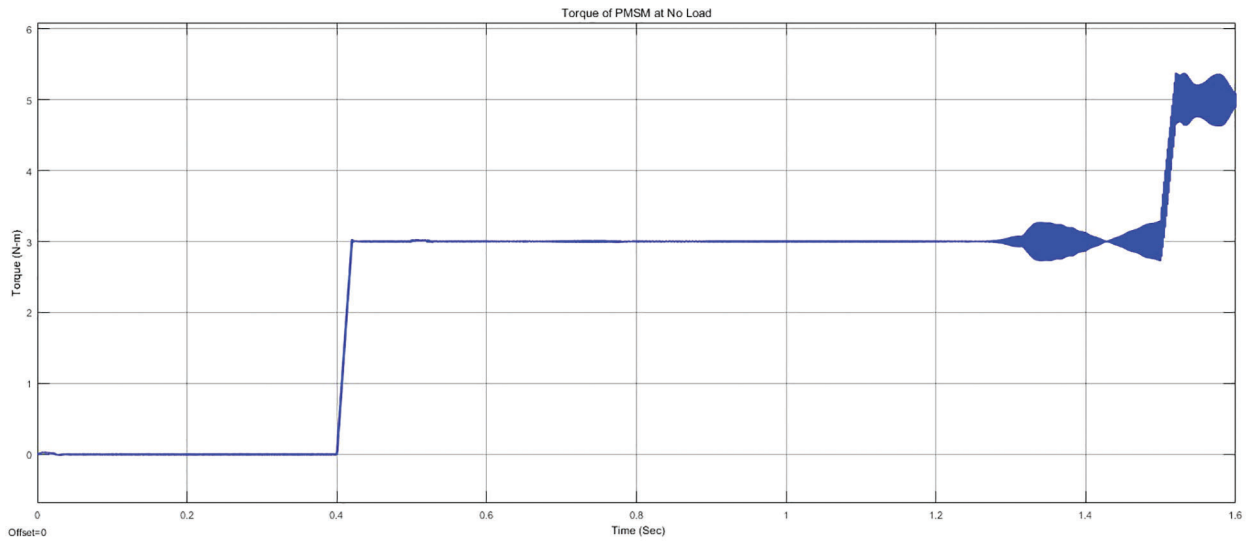
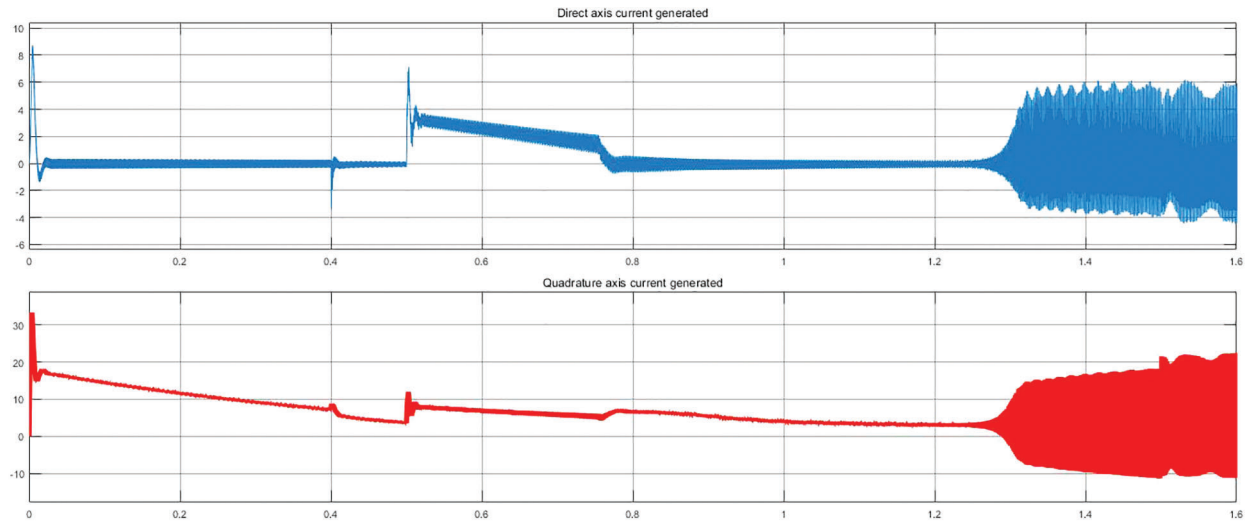
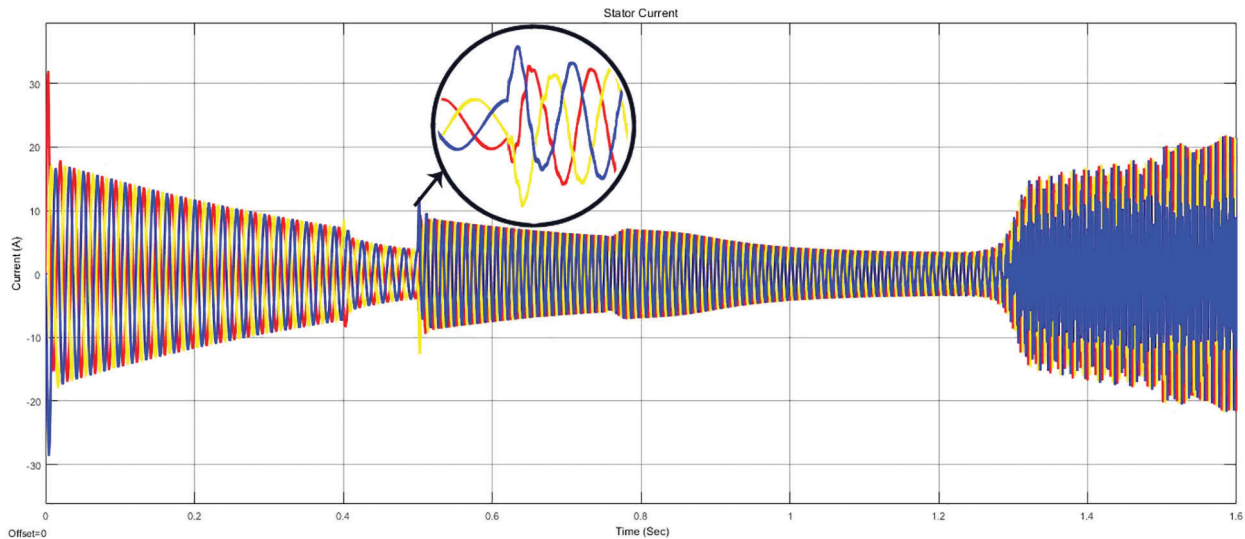


Figure 13: Torque waveform under loaded condition





**Figure 14:** Current waveform of d and q axis under loaded condition



**Figure 15:** Stator current waveform of SPMSM under loaded condition

## 5 Conclusion

A sensorless speed control using SMO for a SPMSM fed by fifteen level inverter has been proposed in this study. MLI has been activated using MCPWM strategy for producing fifteen level voltages. SMO has been modeled for assessing the speed and the rotor position. The projected system is modeled by means of MATLAB/SIMULINK software and has been tested for substantial robustness. The simulations have been carried out for two cases such as no loaded and loaded condition. The results have been extracted under four different speeds. The speed and torque waveforms have been plotted and analyzed. The outcomes evident the efficacy of the projected SMO based sensorless speed organizer. Furthermore, the projected scheme is effective and vigorous against the external disruptions. Concerning the practical evaluation, the working of the controller accompanied by the various observers is under development and its completion is forthcoming.



**Acknowledgement:** The authors with a deep sense of gratitude would thank the supervisor for his guidance and constant support rendered during this research.

**Funding Statement:** The authors received no specific funding for this study.

**Conflicts of Interest:** The authors declare that they have no conflicts of interest to report regarding the present study.

## References

- [1] F. Genduso, R. Miceli, C. Rando and G. R. Galluzzo, "Back EMF sensorless-control algorithm for high-dynamic performance PMSM," *IEEE Transactions on Industrial Electronics*, vol. 57, no. 6, pp. 2092–2100, 2010.
- [2] V. Kumar, P. Gaur and A. P. Mittal, "ANN based self tuned PID like adaptive controller design for high performance PMSM position control," *Expert Systems with Applications*, vol. 41, no. 17, pp. 7995–8002, 2014.
- [3] M. Pacas, "Sensorless drives in industrial applications," *IEEE Industrial Electronics Magazine*, vol. 5, no. 2, pp. 16–23, 2011.
- [4] A. Accetta, M. Cirrincione, M. Pucci and G. Vitale, "Sensorless control of PMSM fractional horsepower drives by signal injection and neural adaptive-band filtering," *IEEE Transactions on Industrial Electronics*, vol. 59, no. 3, pp. 1355–1366, 2012.
- [5] T. O. Kowalska, M. Dybkowski and K. Szabat, "Adaptive Sliding-mode neuro-fuzzy control of the two-mass induction motor drive without mechanical sensors," *IEEE Transactions on Industrial Electronics*, vol. 57, no. 2, pp. 553–564, 2010.
- [6] M. Rho and S. Kim, "Development of robust starting system using sensorless vector drive for a microturbine," *IEEE Transactions on Industrial Electronics*, vol. 57, no. 3, pp. 1063–1073, 2010.
- [7] J. Beerten, J. Verwekken and J. Driesen, "Predictive direct torque control for flux and torque ripple reduction," *IEEE Transactions on Industrial Electronics*, vol. 57, no. 1, pp. 404–412, 2010.
- [8] T. O. Kowalska and M. Dybkowski, "Stator-current-based mras estimator for a wide range speed-sensorless induction-motor drive," *IEEE Transactions on Industrial Electronics*, vol. 57, no. 4, pp. 1296–1308, 2010.
- [9] Z. Wang, Y. Zhang and H. Fang, "Neural adaptive control for a class of nonlinear systems with unknown deadzone," *Neural Computing and Applications*, vol. 17, no. 4, pp. 339–345, 2008.
- [10] C. Lv, Y. Liu, X. Hu, H. Guo, D. Cao *et al.*, "Simultaneous observation of hybrid states for cyber-physical systems: A case study of electric vehicle powertrain," *IEEE Transactions on Cybernetics*, vol. 48, no. 8, pp. 2357–2367, 2018.
- [11] C. Lv, Y. Xing, J. Zhang, X. Na, Y. Li *et al.*, "Levenberg-marquardt backpropagation training of multilayer neural networks for state estimation of a safety-critical cyber-physical system," *IEEE Transactions on Industrial Informatics*, vol. 14, no. 8, pp. 3436–3446, 2018.
- [12] Y. Xing, C. Lv, H. Wang, D. Cao, E. Velenis *et al.*, "Driver activity recognition for intelligent vehicles: A deep learning approach," *IEEE Transactions on Vehicular Technology*, vol. 68, no. 6, pp. 5379–5390, 2019.
- [13] Y. Mei, K. Sun and Y. Shi, "A 2-D fuzzy logic based MRAS scheme for sensorless control of interior permanent magnet synchronous motor drives with cyclic fluctuating loads," *Chinese Journal of Electrical Engineering*, vol. 1, no. 1, pp. 85–91, 2015.
- [14] Y. Zhao, W. Qiao and L. Wu, "Improved rotor position and speed estimators for sensorless control of interior permanent-magnet synchronous machines," *IEEE Journal of Emerging and Selected Topics in Power Electronics*, vol. 2, no. 3, pp. 627–639, 2014.
- [15] J. Yan, H. Lin, Y. Feng, X. Guo, Y. Huang *et al.*, "Improved sliding mode model reference adaptive system speed observer for fuzzy control of direct-drive permanent magnet synchronous generator wind power generation system," *IET Renewable Power Generation*, vol. 7, no. 1, pp. 28–35, 2013.
- [16] B. W. Harini, A. Subiantoro and F. Yusivar, "Stability analysis of MRAS speed sensorless control of permanent magnet synchronous motor," in *Proc. Int. Conf. on Sustainable Energy Engineering and Application (ICSEEA)*, Jakarta, Indonesia, pp. 34–40, 2017.



- [17] O. C. Kivanc and S. B. Ozturk, "Sensorless PMSM drive based on stator feedforward voltage estimation improved with mras multiparameter estimation," *IEEE/ASME Transactions on Mechatronics*, vol. 23, no. 3, pp. 1326–1337, 2018.
- [18] A. A. Alsakati, C. A. Vaithilingam, J. Alnasseir and A. Jagadeeshwaran, "Simplex search method driven design for transient stability enhancement in wind energy integrated power system using multi-band PSS4C," *IEEE Access*, vol. 9, pp. 83913–83928, 2021.
- [19] A. Jagadeeshwaran, S. Vijayshankar, N. Kannan and C. V. Aravind, "Limited angle BLDC for scan mirror application in space satellite system," *IEEE Aerospace and Electronics Systems Magazine*, vol. 31, no. 6, pp. 24–32, 2016.
- [20] A. Jagadeeshwaran, S. Padma, S. Vijay Shankar, V. M. Periyasamy and P. Selvakumar, "Development of limited angle brushless torque motor control drive for scan mirror mechanism," *International Journal of Engineering and Technology*, vol. 5, no. 5, pp. 3907–3913, 2014.
- [21] D. Selvam, S. Subbaian, B. Ananthan and T. Rameshkumar, "T-Source Inverter-based sensorless speed control for permanent magnet synchronous motor," *Journal of Testing and Evaluation*, vol. 48, no. 2, pp. 1745–1768, 2018.